A Validity Study for Perfusion Measurements in the Capillary System

Constantin Heck, Erik A. Hanson,
Arvid Lundervold, Jan Modersitzki, Alexandre Malyshev, Erlend Hodneland
(random order)

Sunday 17th May, 2015

1 Introduction

Quantitative medical measurements based on tracer kinetic models is an important field both in research and in clinical practice [1, 2, 3]. In the present work, we focus on mathematical models for estimating blood perfusion in the brain (cerebral blood flow, CBF) from contrast-enhanced dynamic MR imaging data. Still, the theory on tracer dynamics covered here will also be of relevance in general perfusion studies using other image modalities.

While hardware limitations in medical imaging for decades have confined studies to only handle larger tissue regions or full organs, modern MR technology and voxel based analysis give rise to aspirations about detailed perfusion maps with millimeter precision. Examples of estimated parameter maps are found in i.e. [?]. The quantitative perfusion maps (and other parameter maps arising from tracer kinetic modelling) can be combined with anatomical information, and the maps have proven to be of particular value in e.g. stroke studies for localization of trauma [?]. Among the physiological parameters obtainable from tracer kinetic models, CBF has proven to be particularly difficult to reliably describe on a voxel-basis [4]. In several studies, CBF is therefore only reported in relative values and the corresponding parameter maps are mostly used in a qualitative manner [5]. The methodological limitations in perfusion estimations are caused both by issues in the numerical implementation, but also by over-simplified dynamic models. It is has been widely studied how delay and dispersion of the contrast bolus between the AIF and the voxel as well as assumptions about directional flow [6, 7] effects the perfusion estimation. In [7], a mathematical theory for voxelwise perfusion is introduced and proposed as an alternative to the classical ROI (region of interest) based models for perfusion. In this work, we will use some of the same physical concepts introduced for voxelwise perfusion, and relate them to the classical ROI based perfusion models. We will

further discuss limitations of classical models applied voxel wise, and study their validity in an unstructured flow field. The pharmacokinetic models, and how they behave under different ROI/voxel sizes and shapes, are analyzed mathematically and evaluated within a synthetic flow field. A mathematical framework is also derived, in which the medical notion of perfusion can be understood in a physically more precise manner.

Evaluation of perfusion models using a synthetic flow field is also performed in i.e. [8]. Here, the synthetic model is based on solution of Navier-Stokes equations within the arterial system and the effect of dispersion is studied. In the present work, we model the contrast agent (CA) propagation through a small section of the capillary system. Both these approaches require several clarifying assumptions on flux and propagation. In pharmacokinetic analysis it is often assumed that each ROI (voxel) is an autonomous system that can be modeled by standard pharmacokinetic theory [?]. As in [8], we study CA propagation through a larger area with a highly developed capillary/arterial system and thereby consider a range of connected problems where each voxel can be regarded as an inlet for the surrounding voxels. This more accurately mimics the nature of blood flow in the tissue. Unlike Calamante et al. [8] we also distinguish between scalar perfusion maps, describing flow normalized over a volume, and the physical, vector valued flux field, describing flow normalized over a surface area.

The rest of this paper is arranged as follows: In Section 2, we outline classical methods for perfusion estimation and discuss two widespread solution methods. In Section 3 we describe how a synthetic flow field in the capillary system can be modelled using simple models valid within porous media. We also discuss mathematical similarities between the flow field models and the classical theory outlined in Section 2. Some missing sections here? In Section **??** we evaluate the performance of classical models by applying them to the synthetic flow field. The results and concluding remarks are summarized in Section 6.

2 Classical Models for perfusion

Classical theory for pharmacokinetic modelling is used to recover CBF, cerebral blood volume (CBV), as well as mean transit times (MTT) from data displaying propagation of a contrast agent through the tissue. The so-called deconvolution model (DM) is used in vast amount of publications [9, 10, 11, 12, 13]. Restoration of CBF yields reasonable results [?], however validation is a problem as ground-truth CBF is hard to determine. Validation of novel implementations is usually done in the so-called *inverse crime* setting. This means that the forward model used to generate data and the backward model to reconstruct parameters are similar, if not identical. However, the physical validity of the model can still be questionable. Another model for perfusion which has been used for restoring CBF and MTT is the so-called maximum slope model (MS) [14, 15]. The maximum slope model only considers early time points and it has been shown to exhibit advantages over the deconvolution model especially if uptake curves are degraded in the late phase [10]. However, since it relies on point-wise estimates, application to real

data is nevertheless difficult and prone to noisy measurements. Also, the maximum slope model inherently assumes that no outflow takes place when the AIF peaks (see Sec. 2.2). This assumption is questionable for arbitrary, maybe pathological tissue with possibly prolonged MTT [?].

The classical perfusion models consider the tracer concentration $C(t)$ within a defined compartment, with a compartmentalisation ranging from voxels to entire organs. On the other hand, a field model always describes the tracer concentration locally as $C(x,t)$. As a issue on notation, when classical models are discussed the tracer concentration refers to a spatial average $C(t) = \overline{C}(\Omega_i, t)$ where Ω_i can be compartments ranging from single voxels to larger ROIs.

Following [13], we now briefly present the common theoretical basis of the two models. Let Ω_i be a control volume with one inlet and one outlet and let $C(t)$ denote the average CA concentration within Ω_i at timepoint t. Let us furthermore assume linearity and stationarity What is linear and what is stationary? of CA in- and outflux with proportionality constants $Q_\mathrm{a}, Q_\mathrm{v}$ [$\mathrm{mm}^3/\mathrm{s}/\mathrm{mm}^3$]. These assumptions lead to the differential equation $C'(t) = Q_\mathrm{a} c_\mathrm{a}(t) - Q_\mathrm{v} c_\mathrm{v}(t)$, reflecting mass balance of the tracer. Here $c_\mathrm{a}, c_\mathrm{v}$ are the CA concentrations at the inlet and outlet of Ω_i. Assuming incompressibility of flow leads to $Q_\mathrm{a} = Q_\mathrm{v}$ and hence we obtain the general form

$$C'(t) = Q_\mathrm{a} \left(c_\mathrm{a}(t) - c_\mathrm{v}(t)\right). \tag{1}$$

In the next step, the deconvolution model and the maximum slope model are diverging based on different assumptions.

2.1 The Convolution Model: Theory and Implementation

For the deconvolution model it is assumed that there is a probability distribution of transit times $h(t)$ through Ω_i. This leads to

$$c_\mathrm{v}(t) = (h * c_\mathrm{a})(t) := \int_0^t c_\mathrm{a}(s) h(t-s)\,\mathrm{d}s. \tag{2}$$

Combining this with (1) yields $C'(t) = Q_\mathrm{a} c_\mathrm{a}(t) - Q_\mathrm{a}(h * c_\mathrm{a})(t)$. Integrating this equation and using basic properties of the convolution one obtains

$$C(t) = (I * c_\mathrm{a})(t). \tag{3}$$

Here the *impuls-response function* I is defined as $I(t) := Q_\mathrm{a}(1 - \int_0^t h(s)\,\mathrm{d}s)$, and it fulfills the following properties:

- $I(0) = Q_\mathrm{a}$,
- I is monotonously decreasing,
- $I \geq 0$.

The task of identifying $I(t)$ given a tissue curve $C(t)$ and an arterial input function $c_{\mathrm{a}}(t)$ is a deconvolution problem. If $I(t)$ is recovered, Q_{a} can subsequently be estimated as $Q_{\mathrm{a}} = \max_t I(t)$. There are several methods to perform the deconvolution. A standard approach using Fourier-based algorithms is sensitive to the presence of noise [9, 16]. Another class of deconvolution algorithms gaining increasing attention are based on Bayesian modeling [17, 18]. Recent evaluations are showing good performance [19], however the numerical handling is still difficult since complex and error-prone numerical integration has to be performed. The most popular among deconvolution algorithms are based on singular value decomposition (SVD) [9]. These algorithms have shown to be robust for a reasonable noise level. Also, they can be easily adapted to be robust against delays in tracer arrival using block-circular structures (bSVD cf. [20]). In order to identify the impuls-response function $I(t)$ from simulated data, we hence decided to use the bSVD model as proposed in [20].

If we make the assumption of Ω_i as a well-mixed compartment where $C(t) = CBV\, c_{\mathrm{v}}(t)$ for a $0 \leq CBV \leq 1$, equation (1) reduces to the initial value problem

$$\begin{aligned} (CBV\, c_{\mathrm{v}})' &= Q_{\mathrm{a}} c_{\mathrm{a}} - Q_{\mathrm{a}} c_{\mathrm{v}}, \\ c_{\mathrm{v}}(0) &= 0, \end{aligned}$$

where we also assume no tracer within the compartment for $t = 0$.

Letting $\mathrm{MTT} := Q_{\mathrm{a}}/CBV$ yields the solution

$$C(t) = Q_{\mathrm{a}} \int_0^t e^{-(t-s)/\mathrm{MTT}} c_{\mathrm{a}}(s)\, \mathrm{d}s \tag{4}$$

with residue function $R(t) = e^{-t/\mathrm{MTT}}$.

2.2 The Maximum Slope Model

In the MS model it is assumed that at the beginning when c_{a} peaks, only a negligible amount of CA is leaving the system (cf. [15]). For this time interval equation (1) reduces to

$$C'(t) = Q_{\mathrm{a}} c_{\mathrm{a}}(t), \tag{5}$$

in case one can see that if c_{a} has a maximum, also C' must have a maximum since stationarity in Q_{a} is assumed. Hence, it holds that

$$Q_{\mathrm{a}} = \frac{\max_t C'(t)}{\max_t c_{\mathrm{a}}(t)}. \tag{6}$$

3 A Synthetic Model for Capillary Perfusion

Structurally, the model-assumptions for both classical methods presented in Section 2 are similar. The validity of both methods rely on a ROI having only one inlet and one outlet, and that the CA concentration is well mixed within the entire compartment. In fact, this assumption is questionable when we describe CA propagation through a larger area with a highly developed capillary system. For this type of model system we expect instead a set of coupled equations where each voxel can be regarded as an inlet for surrounding voxels. Hence, in order to make a realistic synthetic model for capillary flow, we decided to describe the CA propagation as a spatially coupled transport process. This synthetic field model is used for validation of the classical ROI based models for perfusion.

Since the CA transport itself is driven mainly by blood flow, we will describe a simple model for the blood flow through capillary tissue in Section 3.1. Within the porous capillary system we expect the blood flow to be driven mainly by pressure differences as modelled by Darcy's law [?]. Traditional tracer kinetic modelling is using volume normalized fluid flow with units [$\mathrm{mm}^3/\mathrm{s}/\mathrm{mm}^3$] as a quantity to describe fluid transport. The concept of volume normalized fluid flow is discretization dependent, and for the current flow simulations we instead use the vector valued surface fluid flux $q = q(x)$ with units [$\mathrm{mm}^3/\mathrm{s}/\mathrm{mm}^2$], in agreement with geoscience and reservoir simulation theory. The fluid flux is a vector field describing the volume of fluid per unit time flowing across a sliced unit area of the sample. A model to convert vector valued flux to scalar valued perfusion with units [$\mathrm{mm}^3/\mathrm{s}/\mathrm{mm}^3$] will be introduced in Section 3.4. The tracer flux $J(x,t)$ [$\mathrm{mmol}/\mathrm{s}/\mathrm{mm}^2$] is assumed to be a product of the fluid flux and the CA concentration, $J(x,t) = c(x,t)q(x)$. Apart from the normalization with respect to surface, the assumptions of linearity and stationarity in the fluid flux are in complete agreement with standard pharmacokinetic modeling [13]. A detailed description of modeling of the blood flow can be found in Section 3.1.

Another ingredient from porous media flow is the introduction of the porosity ϕ $\mathrm{mm}^3/\mathrm{mm}^3$ for $0 \leq \phi \leq 1$. The porosity describes which fraction of a control volume is accessible for blood. Comparing with pharmacokinetic modeling, the porosity directly translates to the cerebral blood volume (CBV).

We will now describe the construction of the digital phantom in detail.

3.1 Modelling the Capillary Blood Flow

We model the blood flow as a fluid flow through a porous medium. The fluid density ρ has units [$\mathrm{mg}/\mathrm{mm}^3$] and is denoted by $\rho = \rho(x,t)$. The flux q [$\mathrm{mm}^3/\mathrm{s}/\mathrm{mm}^2$] as well as the porosity ϕ (with $0 \leq \phi \leq 1$) are assumed to be stationary and hence independent of time. Fluid entering and leaving the system is described by a source- and sink term

$\tilde{Q} = \tilde{Q}(x)$ with units mg/s/mm^3. The continuity equation describing conservation of fluid mass states

$$\frac{\partial(\phi\rho)}{\partial t} + \nabla \cdot (\rho q) = \tilde{Q}. \tag{7}$$

Furthermore, assuming that the fluid flow is steady-state and that the density of blood ρ is constant in space, we obtain

$$\nabla \cdot q = \frac{\tilde{Q}}{\rho}. \tag{8}$$

In order to scale away the density ρ we define another source term Q with units mm^3/s/mm^3 having the relation $\tilde{Q} := Q\rho$, thus transforming (8) into

$$\nabla \cdot q = Q \tag{9}$$

where the right hand side is a volume normalized fluid flow, only non-zero within the source or the sink locations. Elsewhere, (9) is concurrent with divergence free flow of an incompressible fluid.

Low velocity fluid flux in porous media is described by Darcy's law [?]

$$q = -\frac{\mathbf{k}}{\mu}\left(\nabla p + \rho g \nabla z\right). \tag{10}$$

Here g is the gravitational acceleration, $\mathbf{k}$ [mm^2] is the permeability tensor, z is the spatial position along the gravitational field, p [kPa] is the pressure, and $\mu = \mu(x)$ [kPa·s] is the viscosity of the fluid. For the current synthetic model, the flux field is chosen to be perpendicular to the gravitational field and the gravitational term can thereby be discarded,

$$q = -\frac{\mathbf{k}}{\mu}\nabla p. \tag{11}$$

Equations (9) and (11) can be combined, and further it is assumed that k is a symmetric and positive definite tensor such that $\mathbf{k}_{ii} = k$, and zero otherwise. This yields the following elliptic partial differential equation in the pressure-field p,

$$\left| \begin{array}{ll} \nabla \cdot \left(-\frac{k}{\mu}\nabla p\right) = Q & x \in \Omega, \\ n \cdot \nabla p = 0 & x \in \partial\Omega \end{array} \right| \tag{12}$$

where we also added Neuman boundary conditions reflecting zero fluid flux $q(x)$ across $\partial\Omega$. Here, $\partial\Omega$ denotes the boundary of Ω and n the outward unit normal vector. Note that (12) defines a solution which is only unique up to constant [21]. After solving (12), the flux field can be computed according to (11) from the obtained pressure map.

3.2 Modelling Indicator Dilution in the Flux Field

This section describes how the CA propagates in the tissue as it is dissolved in the evolving fluid. We assume that the CA is entering the domain along with the fluid flowing in via the source, and similarly extracted at a sink. The resulting concentration map is a simulation of the CA concentration one would observe within MRI measurements.

In order to define meaningful continuous contrast agent concentrations, we first describe the average CA concentration in an (arbitrarily) small tissue volume Ω_i where $C_i(t)$ is constant within Ω_i. Assume that V_i is the volume of Ω_i and v_i the the blood volume within Ω_i. By definition, porosity is given by $\phi_i = v_i/V_i$. Let $C_i(t)$ denote the CA concentration in Ω_i with respect to the whole volume V_i at timepoint t. The CA concentration with respect to the blood volume v_i is denoted by $c_i(t)$. From the definition of c_i, C_i and ϕ_i we obtain the relation $C_i(t) = \phi_i c_i(t)$. The rate of change of tracer molecules within the control volume Ω_i can he phrased as

$$\frac{\mathrm{d}}{\mathrm{d}t}\int_{\Omega_i} C_i(t)\,\mathrm{d}x = \int_{\Omega_i} \frac{\mathrm{d}}{\mathrm{d}t}(\phi_i c_i(t))\,\mathrm{d}x = \int_{\Omega_i} \phi_i \frac{dc_i}{dt}\,\mathrm{d}x. \tag{13}$$

where the assumption of stationary ϕ_i was used. Since we expect mainly transport along the vessels and marginal diffusion, the change in tracer mass within Ω_i occurs only from advective flow and the source and sink field Q. Let us write the source- and the sink term as $Q = Q_{\mathrm{si}} + Q_{\mathrm{so}}$ where $Q_{\mathrm{si}} < 0$ is the sink and $Q_{\mathrm{so}} > 0$ is the source. Both are assumed to be zero everywhere except at in the respective source and sink locations. Note that $\int_\Omega Q\,\mathrm{d}x = 0$. The change in contrast agent at time point t can hence be written as

$$-\int_{\partial\Omega_i} c_i(t)(q_i \cdot n)\,\mathrm{d}s + \int_{\Omega_i} c_{\mathrm{a}}(t) Q_{\mathrm{so}}\,\mathrm{d}x + \int_{\Omega_i} c_i(t) Q_{\mathrm{si}}\,\mathrm{d}x, \tag{14}$$

where n is the outward unit normal on $\partial\Omega_i$. Furthermore, $c_{\mathrm{a}}(t)$ [mmol/mm^3] describes the CA concentration entering the system at the source. In standard pharmacokinetic modeling, c_{a} is referred to as the arterial input function (AIF). From the principle of conservation of tracer molecules, equations (13) and (14) must balance such that

$$\int_{\Omega_i} \phi_i \frac{dc_i}{dt}\,\mathrm{d}x + \int_{\partial\Omega_i} c_i(t)(q_i \cdot n)\,\mathrm{d}s = \int_{\Omega_i} c_{\mathrm{a}}(t) Q_{\mathrm{so}}\,\mathrm{d}x + \int_{\Omega_i} c_i(t) Q_{\mathrm{si}}\,\mathrm{d}x. \tag{15}$$

Now, let the contrast agent concentrations be a continuous function of space and time, $C(x,t), c(x,t)$, and $\phi(x), q(x)$. Equation (15) is then consistent with the continuity equation on local form

$$\left|\begin{array}{ll} \phi\dfrac{\partial c}{\partial t} + \nabla\cdot(cq) = c_{\mathrm{a}}Q_{\mathrm{so}} + cQ_{\mathrm{si}} & x \in \Omega,\ t > 0, \\ c(x,t) = 0 & x \in \Omega,\ t = 0. \end{array}\right| \tag{16}$$

where we also added the initial value $c(x,0) = 0$ to ensure uniqueness. Equation (16) is a linear transport equation in $c(x,t)$. Assuming that ϕ is Lipschitz continuous and that $Q_{\mathrm{so}}, Q_{\mathrm{si}}, c_{\mathrm{a}}$ are continuous functions, we can follow that q, as the solution of (12), is also Lipschitz continuous. In this case (16) has a unique local solution [21].

3.3 Relating the Classical and the Synthetic Model

Here is still some motivation missing.

In order to test the standard models for their abilities to restore CBF and CBV, we need to convert the flux q with units $\mathrm{mm}^3/\mathrm{s}/\mathrm{mm}^2$ to perfusion P with units $\mathrm{mm}^3/\mathrm{s}/\mathrm{mm}^3$. A method to do that will be presented in Section 3.4. In Section 3.5 we will give a proof that the porosity CBV can be estimated from the standard relationship CBV $= \left(\int_0^\infty C(x,s)\,\mathrm{d}s\right) / \left(\int_0^\infty c_\mathrm{a}(s)\,\mathrm{d}s\right)$.

3.4 Converting Flow to Perfusion

The model described in (11) - (12) uniquely determines the flux field $q(x)$. However, in pharmacokinetic modeling the parameter of interest is usually the CBF, which we will denote by $Q(x)$ as the voxel wise field of perfusion. However, it is not obvious how to transform a vector flux field $q(x)$ into a scalar perfusion field $Q(x)$. There are at least two differences between $q(x)$ and $Q(x)$. First, the flux is a vector field and the perfusion is a scalar field. Second, the flux is normalized to a surface area and the perfusion is normalized to a volume. Thus, these to quantities are strictly, mathematically different but still conceptually related. In the following we describe a method for converting flux into perfusion. The other way around, converting perfusion into flux has no obvious incentive since the vector flux field contains both scalar and directional information compared to the scalar perfusion field.

The common understanding of perfusion $Q(x)$ is the amount of blood feeding a tissue volume per unit time, with units $[\mathrm{mm}^3/\mathrm{s}/\mathrm{mm}^3]$. For inter-subject comparison it is common to scale this quantity to normalized perfusion $P(x)$ with units ml/s/100ml. One approach for converting flux into perfusion could be to estimate the perfusion as the total inflow (or outflow) of fluid (e.g. arterial blood) into a control region per unit time, and then normalizing with the entire control region volume. This is a valid approach only if every control region is separated from other control regions and not feeding each other, and this approach is thereby well-founded for an entire organ. Such understanding of perfusion is in line with the theoretical foundation of classical compartment models for perfusion where each control region has its own source of feeding arterial blood, independent of the neighbor regions.

On the other hand, if the control region is a single voxel or a sub-division of an organ with common feeding arterial blood, the classical model assumptions are is violated since the control regions will be fed by their neighbours, and thus becoming a coupled system of flow. Simply summing the total inflow into a voxel and dividing by the voxel volume will strongly over-estimate the perfusion since the normalization would refer to the wrong volume. The problematic issue is that the incoming blood is feeding more ROIs than the current ROI, and the perfusion values thereby become discretization dependent. This phenomenon is demonstrated in Fig. 1 where the volume on the left has the true

perfusion of $Q_1 = F_0/(2V)$ for an incoming flow F_0 [mm^3/s] and distribution volume $2V$ [mm^3]. However, for another discretization as shown in the middle, the perfusion within each of these sub-volumes becomes $Q_2 = F_0/V = 2Q_1$. Taking the average across the two sub-volumes, it is clear that the perfusion is over-estimated with a factor of two. A discretization dependent perfusion value is not desirable, and the perfusion estimate of Q_2 is clearly wrong.

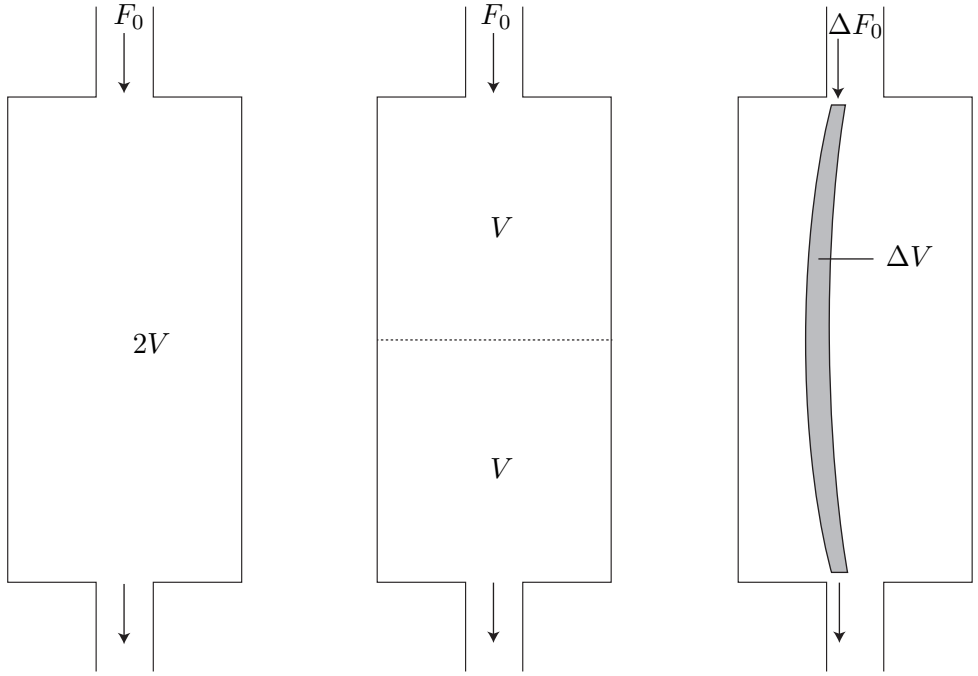

Figure 1: Perfusion within a small volume. Left: A compartment with volume $2V$ is exposed to a flow F_0 [mm^3/s] of fluid. From definition of perfusion, the perfusion within this compartment becomes $Q_1 = F_0/(2V)$. Right: The volume is divided into two smaller compartment (e.g. voxels), and the perfusion for each of the compartments becomes $Q_2 = F_0/V = 2Q_1$. The discrepancy between the two discretizations occurs because the flow is counted twice as it is fed from one voxel to the other. Right: As a solution to the described problem we rather pick out a true distribution volume ΔV (area in this 2D sketch), which is a small area around a given streamline along the centre line of the grey area. This is the true distribution volume (area) which is fed with arterial blood from the incoming fractional flow ΔF_0. The correct perfusion within ΔV is therefore $\Delta F_0/\Delta V$. The entire compartment can further be divided into infinitesimal distribution volumes, thus providing correct voxelwise perfusion values.

The reason for the discrepancy is that Q_2 has been counted twice since the voxels are coupled and we are dividing by the wrong distribution volume. The concept of perfusion has a very precise meaning, as the amount of arterial blood per time unit delivered to a

capillary bed in a biological tissue, and then scaled by the feeding tissue volume. Therefore, the incoming flow must be divided by the total distribution volume that is covered by the fluid streamlines. This formulation coincides with the classical understanding of perfusion, and the correct distribution volume will rather be the volume that the fluid particles within an infinitesimal cross-sectional area around the streamlines are covering. Assuming laminar flow, the streamlines are not crossing each other and we can estimate the true distribution volume that is fed by a given arterial blood flow.

Let us fix a point $y \in \Omega$ and consider the streamline crossing through y. For the time being, denote the flux along this streamline as $q = q(s)$ for a parameterization s along the streamline, noting that the direction of the streamline is identical to the direction of the flux. Let A_ε be a 2-D disc with radius $\varepsilon(s)$, where A_ε is orthogonal to $q(s)$. Thus, the normal vector n of the disc, is parallel to $q(s)$. The volume flow [mm^3/s] over the disc is independent of the position along the streamlines, and can be expressed as

$$F = \int_{A_\varepsilon} (q \cdot n) \, \mathrm{d}A = \int_{A_\varepsilon} \left(q \cdot \frac{q}{\|q\|} \right) \mathrm{d}A \tag{17}$$

for any $0 \leq s \leq L$ where L is the length of the streamline, and thereby for any ε along the streamline. Provided q is continuous along the streamlines, we know $\exists \ \tilde{\varepsilon}, 0 \leq \tilde{\varepsilon} \leq \max_s \varepsilon(s)$, such that the volume V of the tube can be expressed as $V = \tilde{\varepsilon}^2 \pi L$ Hence we can express the perfusion Q_ε for the sub volume V as

$$Q = \frac{F}{V} = \frac{1}{\tilde{\varepsilon}^2 \pi L} \int_{A_{\tilde{\varepsilon}}} \left(q \cdot \frac{q}{\|q\|} \right) \mathrm{d}A. \tag{18}$$

Letting $\tilde{\varepsilon} \to 0$ and using that $F/(\tilde{\varepsilon}^2 \pi) \to \|q\|$ provided q is continuous, yields a locally defined value for the perfusion $Q(y)$

$$Q(y) = \frac{\|q(y)\|}{L}. \tag{19}$$

We note that (18) is valid for any $0 \leq \tilde{\varepsilon} \leq \max_s \varepsilon(s)$ since both F and V are independent of ε, and relation (19) is thereby valid for any position along the streamline. This is an explicit formula for converting flux into perfusion and is later used for evaluation of the classical model for perfusion.

3.5 A Method to Estimate the Porosity

It is known from literature on classical models for perfusion that CBV for the entire compartment can be expressed as

$$CBV = \frac{\int_0^\infty C(t) dt}{\int_0^\infty c_a(t) dt}. \tag{20}$$

where $C(t)$ are the tracer concentration within a well mixed compartment and $c_a(t)$ is the tracer concentration of the arterial input. However, it is not obvious that (20) is valid

also for a continuous field model where the voxels are feeding each other. We will now proof that (20) is nevertheless valid.

Returning to the local definition of fluid tracer concentration as $c(x,t)$, the PDE in (16) is consistent with

$$\phi \frac{\partial c}{\partial t} = -q \cdot \nabla c. \tag{21}$$

for locations x where $Q(x) = 0$. Integrating from t_0 to t_1 results in the model

$$\phi[c(x,t_1) - c(x,t_0)] = -\int_{t_0}^{t_1} q \cdot \nabla c \, \mathrm{d}t. \tag{22}$$

Approaching the limit $t_0 = 0, t_1 = \infty$, using the boundary conditions $c(x,0) = c(x,\infty) = 0$ and defining $E(x) := \int_0^\infty c(x,t)\,\mathrm{d}t$ leads to

$$0 = q \cdot \nabla E(x). \tag{23}$$

We can interpret this equation such that q lies parallel with the level-sets of the function $E(x)$, which means that $E(x)$ is constant along the streamlines of the fluid flow, and thereby also valid when approaching the source $\Omega_Q = \{x : Q(x) \neq 0\}$ along the streamlines:

$$\int_0^\infty c(x,t)\,\mathrm{d}t = \lim_{x \to \Omega_Q} \int_0^\infty c(x,t)\,\mathrm{d}t. \tag{24}$$

Using $C(x,t) = \phi(x)c(x,t)$ we obtain

$$\phi(x) = \frac{\int_0^\infty C(x,t)\,\mathrm{d}t}{\lim_{x \to \Omega_Q} \int_0^\infty c(x,t)\,\mathrm{d}t}. \tag{25}$$

For all practical applications with a source field Ω_Q of limited extension and homogeneous and simultaneous CA input one can replace the denominator by $\int_o^\infty c_a(t)\,\mathrm{d}t$. Equation (25) for porosity then coincides with the classical formula (20) for CBV and is hereby proven analytically also for local estimations of CBV.

4 Numerical Implementations of the Synthetic Model for Capillary Perfusion

In this section we describe how the models were implemented numerically. For simplicity the domain is discretized by a regular cartesian grid of size $n \times n$ with a regular cell-spacing h. The proposed method may be extended for non-regular grids in an analogous fashion.

To solve (12) we used the two-point flux approximation finite volume method (TPFA) [?]. The transport equation (16) was solved by upwinding applied to (15) [?].

4.1 Discretization of the Single Phase Flow Model using TPFA

Equation (12) was solved using the TPFA method widely used in reservoir mechanics [?]. Integrating (12) across a small domain (voxel) $\Omega_i \subset \Omega$ and applying the divergence theorem yields

$$\int_{\partial\Omega_i} -(\lambda \nabla p) \cdot n \, \mathrm{d}s = \int_{\Omega_i} Q \, \mathrm{d}x \tag{26}$$

with conductivities $\lambda := k/\mu$. Defining $\partial\Omega_{ij}$ as the boundary between neighboring voxels Ω_i and Ω_j, only the flux component perpendicular to $\partial\Omega_{ij}$ will drive the flow between these voxels. The component of ∇p pointing along the normal vector of $\partial\Omega_{ij}$ can in terms of cell centered pressure values p_i and p_j be replaced by $\Delta p_{ij} := (p_j - p_i)/h$. Hence, the total flux across the face Γ_{ij} can be approximated by

$$\Delta p_{ij} \int_{\partial\Omega_{ij}} \lambda \, \mathrm{d}s \approx (p_i - p_j) \underbrace{\frac{\lambda_{ij} |\partial\Omega_{ij}|}{h}}_{:=t_{ij}}. \tag{27}$$

Here, λ_{ij} denotes an approximation of the mean conductivity on $\partial\Omega_{ij}$, where λ_{ij} is computed by harmonic averaging from the requirement of continuity in p on the midline of $\partial\Omega_{ij}$. The terms in (27) not depending on the pressure p are collected into the transmissibilities $t_{ij} := |\partial\Omega_{ij}|\lambda_{ij}/h$. Approximating the right hand side of (27) as $\int_{\Omega_i} Q \, \mathrm{d}x \approx Q_i |\Omega_{ij}|$ yields a linear system which can be solved for the pressure p. Due to the Fredholm alternative, we imposed Dirichlet boundary conditions for one voxel within Ω to ensure uniqueness. Note that p, k, Q and μ are defined cell-centered whereas the resulting flux is discretized on a staggered grid, corresponding to the voxel faces.

4.2 Discretization of the Transport Equation

The transport described in (15) was implemented using an upwind Godunov scheme [?]. Let c_{ij} be a cell centered voxel tracer concentration with respect to the fluid volume on the cell face $\partial\Omega_{ij}$ adjacent to voxel i and voxel j, and let n_{ij} be the outer normal vector of $\partial\Omega_{ij}$. Also, the cell staggered fluid flux is represented as a vector q_{ij}. The total CA-flux over the face $\partial\Omega_{ij}$ for any time point was approximated by

$$\int_{\partial\Omega_{ij}} c_{ij}(q_{ij} \cdot n_{ij}) \, \mathrm{d}s \approx \begin{cases} c_i q_{ij,n} |\partial\Omega_{ij}| & \text{if } q_{ij,n} \geq 0, \\ c_j q_{ij,n} |\partial\Omega_{ij}| & \text{if } q_{ij,n} < 0, \end{cases} \tag{28}$$

where $q_{ij,n} = q_{ij} \cdot n_{ij}$ is the normal component of the flux across $\partial\Omega_{ij}$. Keeping track of in- and outflow for each voxel yields an explicit discretization scheme to set up the transport simulation. We used a time step of $\Delta t = 0.002s$ in a forward Euler time stepping of (15). A conversion of c_i into C_i was performed via the relation $C_i = c_i \phi_i$. The overall concentration map C_i was later used for the inverse problem of restoring CBV and CBF.

We chose a standard arterial input function [9], a gamma-variate [22] function

$$c_{\mathrm{a}}(t) := (t - t_0)^{\alpha} e^{-(t-t_0)/\beta} \tag{29}$$

for $\alpha = 3$, $\beta = 1.5\,\mathrm{s}$ and $t_0 = 0\,\mathrm{s}$.

5 Numerical Experiments and Results

5.1 Parameter settings

Based on (12) and (16) we set up a forward simulation of blood-flow and indicator dilution through the capillary system. An overview of parameter settings used for the numeral simulations are shown in Table 1. Note that total inflow within the source is denoted $F_{so} = \int_\Omega Q_{so}(x)dx$, as well as for the sink $F_{si} = \int_\Omega Q_{si}(x)dx$. We chose an average input perfusion of 50ml/s/100ml, which can be converted into a flow of $F_{so} = 0.83$ ml/s for the domain $\Omega = \{x = (x_1, x_2, x_3) : 0 \leq x_1 \leq 10mm, 0 \leq x_2 \leq 10mm, 0 \leq x_3 \leq 0.1mm\}$.

Table 1: Parameters used in the numerical experiments, optimized for a slab of the capillary system in the human brain. In order to achieve a transparent simulation, permeability was assumed to be isotropic, and both the permeability and porosity were assumed to be constant across the domain.

Description	Type	Symbol	Value(s)	Unit
Fluid flux	Vector	q	-	$\mathrm{mm}^3/\mathrm{s}/\mathrm{mm}^2$
Fluid flow ($q \cdot dA$)	Vector	J	-	mm^3/s
Concentration w.r.t. fluid space	Scalar	c	-	$\mathrm{mmol}/\mathrm{mm}^3$
Concentration w.r.t. Ω_i	Scalar	C	-	$\mathrm{mmol}/\mathrm{mm}^3$
Average perfusion within Ω	Scalar	$\overline{Q}$	50	ml/s/100ml
Volume flow source, derived from $\overline{Q}$	Scalar	F_{so}	0.83	ml/s
Volume flow sink	Scalar	F_{si}	$-F_{so}$	ml/s
Estimated perfusion	Scalar	Q	-	$\mathrm{mm}^3/\mathrm{s}/\mathrm{mm}^3$
Dynamic viscosity blood [23]	Scalar	μ_b	5×10^{-6}	kPa·s
Fluid density blood [24]	Scalar	ρ	1	$\mathrm{mg}/\mathrm{mm}^3$
Permeability	Scalar	k	5×10^{-6}	mm^2
Porosity [20]	Scalar	ϕ	0.05	$\mathrm{mm}^3/\mathrm{mm}^3$
Spatial resolution	Vector	-	$(64, 64, 1)$	-
Physical FOV	Vector	-	$(10, 10, 1)$	mm
Voxel size	Vector	-	$(0.156, 0.156, 1)$	mm

We aimed at creating a transparent synthetic test case and kept all optional parameters as simple as possible. Therefore, permeability and porosity were assumed constant in space and in time. The source term was assigned to the upper left voxel and the sink term was assigned to the lower right voxel.

5.2 Indicator dilution in the porous media and the convolution model

From the porous media model, streamlines were found from tracking within the flux vector field q, a method almost identical to FACT used for DTI (Diffusion Tensor Imaging) for tractography. Both length and position of the streamlines was during the tracking process assigned. The voxel-wise perfusion field Q_i was calculated according to (19) using the computed streamline length and the flux field q from (11). The pressure field, the flux and voxel wise perfusion is displayed in Fig. 2. The flow field visualized in Fig. 2 (b) is vector flux integrated across cell surface, becoming the flow field across surface $\partial\Omega_{ij}$, $J_{ij} = \int_{\partial\Omega_{ij}} qds$ [mm^3/s].

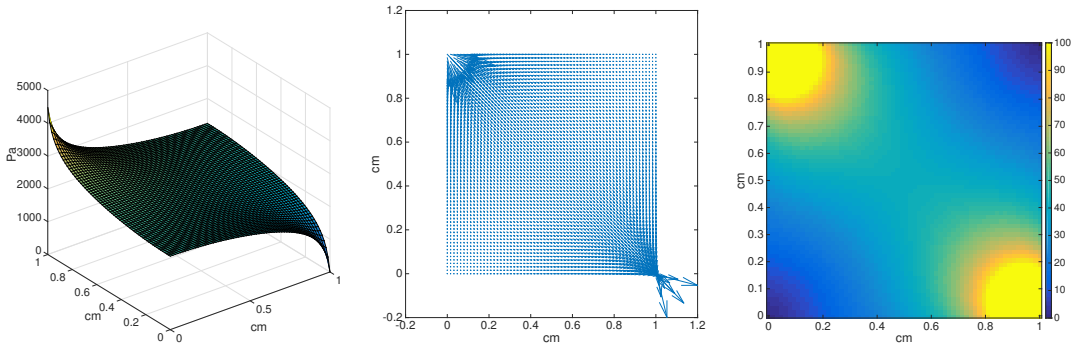

(a) Pressure field p (b) Flow field J_{ij} (c) Perfusion field P_i.

Figure 2: Porous media (PM) flow model with a source in the upper left corner and a sink in the lower right corner. (a) Pressure field [Pa] from solving the linear system in (12) , (b) Vector valued flow field $J_{ij} = \int_{\partial\Omega_{ij}} qds$ [mm^3/s], (c) Voxelwise perfusion P_i [ml/s/100ml] according to (19).

A map of CA concentrations was computed by two means. (i) First, by simulating the transport equation (15), and (ii) second by the forward convolution model (4): For the transport equation (i), known values of flux, porosity, fluid density, and fluid flow within the source and sink were fed into the equation. We refer to this map as $C_T(x,t)$. For the forward convolution model (ii), the estimated perfusion Q and the porosity was used for the simulations with known values of $Q_a \leftarrow Q_i$. We refer to this map as $C_C(x,t)$. A comparison of the tissue curves between $C_T(x,t)$ and $C_C(x,t)$ at different positions of the tissue can be found in Figure 3.

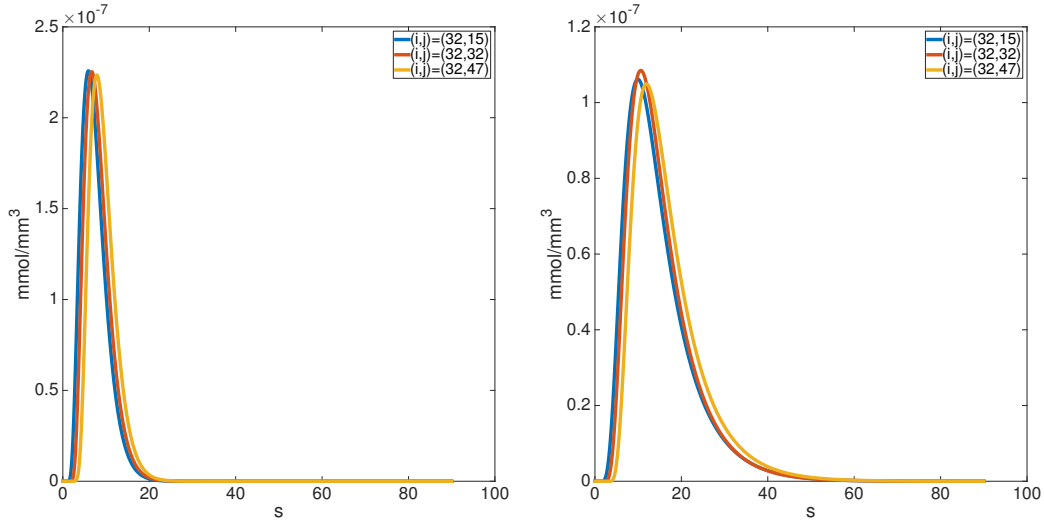

(a) Transport equation $C_T(x,t)$ (b) Convolution model $C_C(x,t)$

Figure 3: Comparison of tissue curves using the transport equation $C_T(x,t)$ (a) and the convolution model $C_C(x,t)$ (b). Curves were sampled in the middle row $i = 32$ and columns $j \in \{15, 32, 47\}$. The convolution model creates a more dispersed signal compared to the transport equation.

5.3 Reconstruction of Perfusion by classical Models

We tested the the convolution based classical model (3) as well as maximum-slope model (6) for their capability to recover the perfusion values. The success of the restoration was measured voxelwise in terms of the relative error of the recovered perfusion with respect to the true perfusion

$$RE := \frac{|Q_{\text{rec}} - Q_{\text{true}}|}{Q_{\text{true}}} \cdot 100\%. \tag{30}$$

Prior to reconstruction, the maps $C_T(x,t)$ and $C_C(x,t)$ of CA in time and space were downsampled to a time-resolution of 0.2 s in order to stay within comparable time sampling existing on modern MR equipment for dynamic imaging. In order to simulate different spatial resolutions of the scanning process, the data was averaged using different block-sizes ranging from $(1,1)$ to $(64,64)$. Results are displayed in Figure 4 as well as in Table 2. Impulse response function reconstructed from the transport equation are displayed in Figure 5.

Table 2: Relative error RE (%) for reconstructing perfusion Q. Relative error was computed block-wise as $RE = |Q_{\text{rec}} - Q_{\text{true}}|/Q_{\text{true}} \cdot 100\%$. Displayed is the median RE. Both reconstruction models MS and bSVD are able to restore the perfusion for the entire domain, but fail for smaller block sizes. The bSVD model is able to restore the voxel size perfusion when it was generated by the convolution model.

	Reconstruction	Block Size (voxels)			
Forward data	model	(1,1)	(5,5)	(10,10)	entire domain
Transport equation	MS	170.09	165.03	158.57	2.65
	bSVD	859.06	768.58	664.84	1.25
Convolution model	MS	23.20	24.26	25.75	37.96
	bSVD	2.43	4.27	8.80	20.72

Table 3: Relative error RE (%) for reconstructing CBV. The CBV was computed according to (20). Relative error was computed block-wise as $RE = |\phi_{\text{rec}} - \phi_{\text{true}}|/\phi_{\text{true}} \cdot 100\%$. Displayed is the median RE. The reconstruction errors are small for all block sizes and both forward models.

	Block Size (voxels)			
Forward data	(1,1)	(5,5)	(10,10)	entire domain
Transport equation	$4.37 \cdot 10^{-5}$	$4.37 \cdot 10^{-5}$	$4.37 \cdot 10^{-5}$	$4.37 \cdot 10^{-5}$
Convolution model	$1.94 \cdot 10^{-2}$	$1.93 \cdot 10^{-2}$	$2.12 \cdot 10^{-2}$	1.13

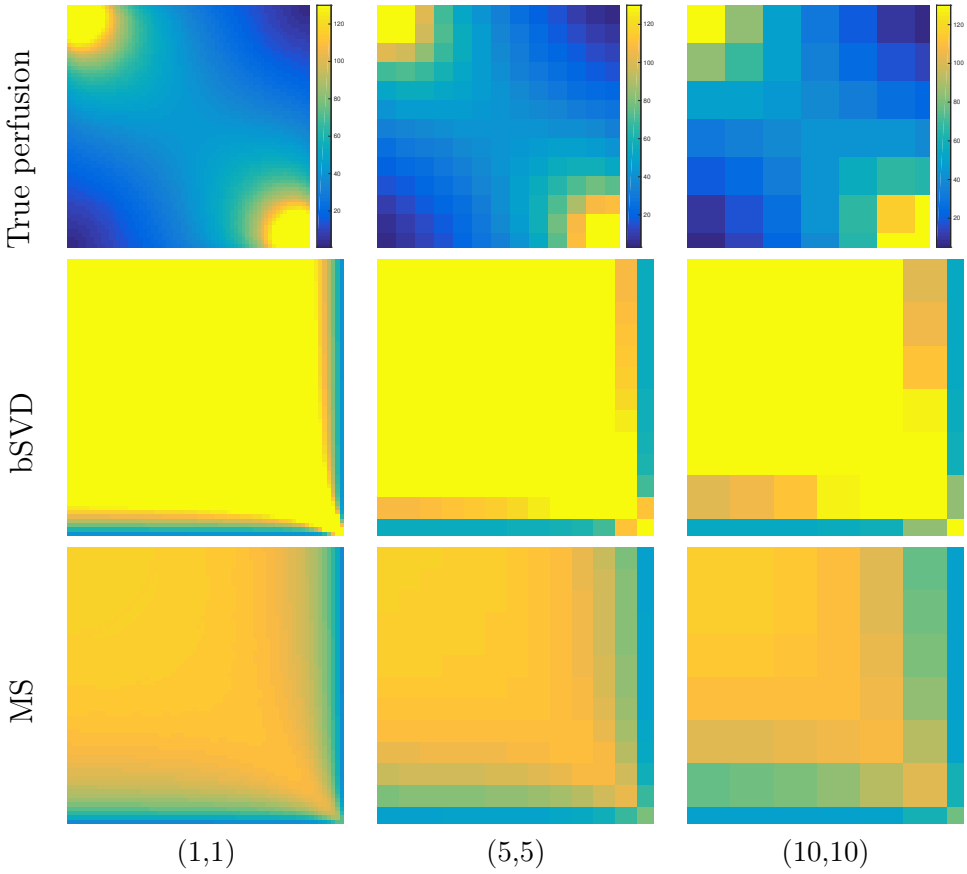

Figure 4: Restoring the perfusion for different levels of discretization, displayed within the columns. Block size in voxels is shown in brackets. All results are given in ml/min/100ml. First Row: Ground-truth perfusion (cf. Section 3.4). Second Row: Perfusion as estimated by bSVD. Third Row: Perfusion as estimated by the MS model. Both reconstruction methods fail in restoring the true perfusion, as reflected in the relative errors of Table 2.

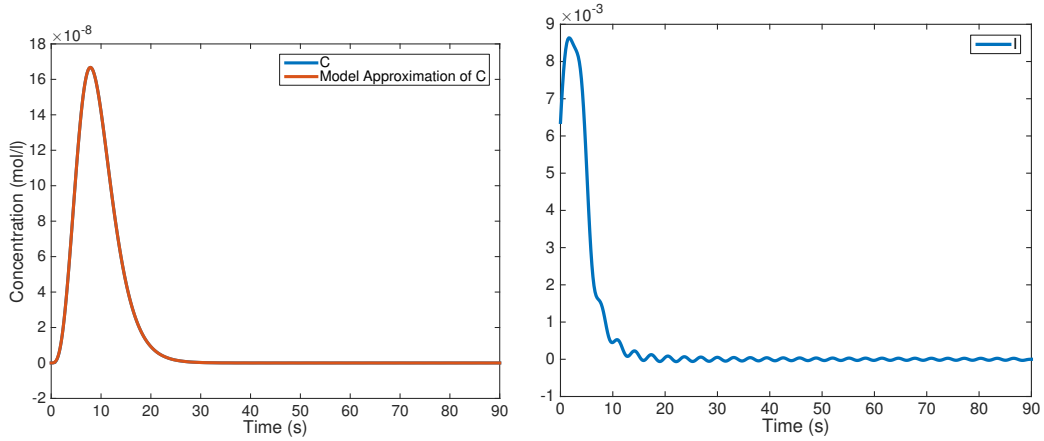

(a) Entire Domain, $C_T(x,t)$

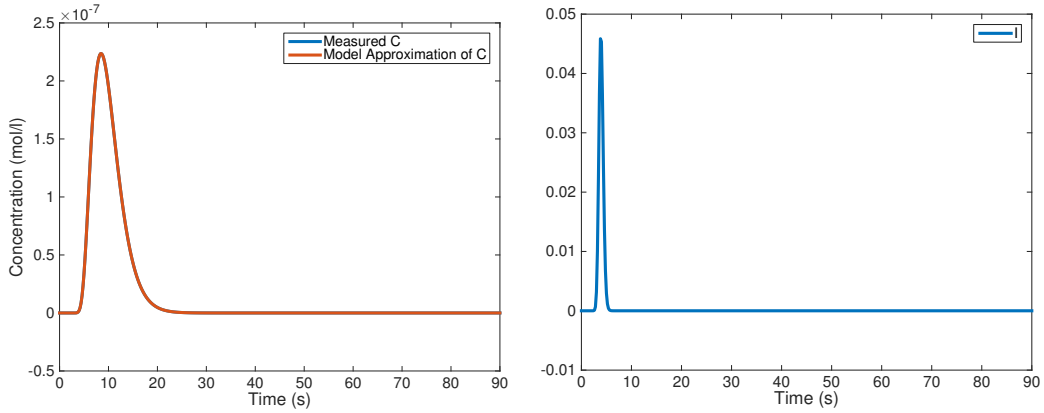

(b) Inside the capillary bed, $C_T(x,t)$ at $(i,j) = (50,50)$

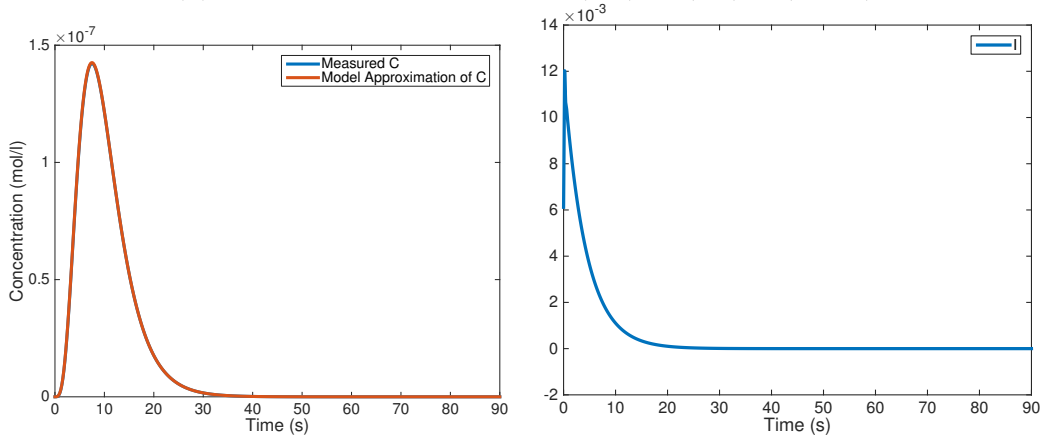

(c) Inside the capillary bed, $C_C(x,t)$ at $(i,j) = (50,50)$

Figure 5: Deconvolution by bSVD. First row: Results of bSVD applied to the map $C_T(x,t)$ generated with the transport equation (15) using block-size (64,64) (i.e. entire domain). Second row: Results of bSVD applied to a single voxel of $C_T(x,t)$ in the inside of the domain. Third row: Results of bSVD applied to a single voxel of the convolution data $C_C(x,t)$ in the inside of the domain. In all cases the model restored the measured concentration curves perfectly. Left to right: Shown is reconstructed concentration $c(t)$ (left) and the impuls-response function I(t) (right).

6 Discussion

Accurate measurements of CBV, CBF and MTT within the brain can provide substantial input in clinical decision making. Originally, the classical 1-C models for these parameters were developed for larger ROIs, and their validity for usage in field models has not properly been established. In this work we have developed a porous media simulator for simulating blood flow within a slab of the capillary system. From the obtained flux field, we generate a perfusion map that was used to create two data sets of propagating concentration agent. The first approach is based on solving a transport equation, where every voxel acts as an arterial input to its neighbours. The other approach is based on a forward convolution model, where every voxel is exposed to the same arterial input function. The latter data set was mainly used to validate the numerical stability of the deconvolution methods, while the first data set was meant to represent a realistic data set as it can be obtained from a MR examination.

Considering the data set created from the transport equation, the results presented in Table 2 indicate low errors or $RE \leq 2.6\%$ of both the MS and the bSVD model for restoring the perfusion when applied to the entire domain. This is in good agreement with assumptions for classical models, like well-mixed fluids within the compartment, and where only the average tracer concentration is considered. Thus, these results support the usage of classical compartment models for whole organs with only one inlet and one outlet.

However, the reconstruction of perfusion using MS and bSVD fails to a large extend with relative errors put o 859% for all other block sizes that the entire domain, and apparently increasing for smaller block size. This observation indicates that classical models for reconstructing perfusion are not valid for a situation where the true arterial input is not the practically correct arterial input for smaller computational units. In this respect, assumptions of the classical models are violated as the arterial input will be dispersed in unpredictable ways on the way from the inlet to the computational unit.

Considering the data set created from convolution, from the same table it is clear that the bSVD model for deconvolution has a low error of 2.43% for voxel wise reconstruction. This result is closely related to the previously described "inverse-crime" where we used the same model for constructing the data as for reconstruction. However, in our case it provides evidence that the deconvolution algorithm used, the bSVD, is numerically stable, and that errors in true perfusion are unlikely to arise from numerical instabilities of the deconvolution. This conclusion is also supported by Fig. **??**, where the measured and the restored concentration curves are more or less identical for various block sizes and various input data. However, despite the success of restoring the concentration curves, the usage of a model in an "inverse-crime" settings can not be used to support the physical validity of the model, only the numerical stability of the deconvolution, in this case.

Interestingly, the MS model fails in restoring the perfusion for all block sizes of the forward convolution data. The reason for this is probably that within the MS model

there is an assumption of no output of CA as the arterial input peaks. This assumption is clearly violated as the forward convolution model assumes an instantaneous transport of CA both into as well as out of the domain since the compartment is assumed to be well mixed.

Regarding the CBV estimations, one can observe from Table 3 that both data sets $C_T(x,t)$ and $C_C(x,t)$ could successfully be used to restore the CBV. Various block sizes also had little impact on the results. These results are in well agreement with the analytical proof of CBV in Section 3.5, that this expression is valid for entire organs as well as for single voxels. Thus, these results support the usage of (20) for computing the CBV with high accuracy for any type of block size, including single voxels.

In light of our current findings we want to put focus on the usage of classical compartment models for voxel wise perfusion in the brain. Our results indicate the classical models should only be used for larger computational units where the arterial input is a good representation of the feeding blood flow. The development of new field models for perfusion is therefore highly demanded, in line with approaches described in [7]. Our results are only valid for one-compartment systems like the brain with an intact blood-brain-barrier. For other organs or pathological situations with a leakage of tracer into the extravascular space, the observed effects described in this work are yet to be discovered.

Apparently, the true perfusion in a brain is unknown, and a gold standard is therefore not accessible for real data on a voxel wise basis. As an alternative, we propose to use simulated data sets as described in this work for benchmarking of new perfusion reconstruction algorithms. Applied to the same data set it it would be easier to compare the performance of different methods.

Concluding, we have proposed a novel method to validate classical models for perfusion analysis. We have shown that within the assumptions of well mixed compartment and a common arterial input, classical models for restoring the perfusion are reliable. However, when sub-dividing the computational units into smaller ROIs, even down to voxels, significant errors are introduced. Furthermore, these errors are not likely to be related to the deconvolution method, but are rather related to violation of the physical model assumptions. In light of these results, future work should include the development of field models for perfusion measurements, taking into account the local constellation and neighbourship of voxels. By these means one could develop reliable models also for voxel wise estimates. In this process it is useful to have benchmarking models for judging reliability of the models. We suggest that our simulated flow model could be used for such comparisons.

References

[1] K. L. Zierler, "Theoretical basis of indicator-dilution methods for measuring flow and volume," *Circ Res*, vol. 10, no. 3, pp. 393–407, 1962.

[2] L. Axel, "Cerebral blood flow determination by rapid-sequence computed tomography: theoretical analysis.," *Radiology*, vol. 137, no. 3, pp. 679–686, 1980.

[3] K. Zierler, "Indicator dilution methods for measuring blood flow, volume, and other properties of biological systems: a brief history and memoir," *Ann Biomed Eng*, vol. 28, no. 8, pp. 836–848, 2000.

[4] K. Kudo, M. Sasaki, K. Yamada, S. Momoshima, H. Utsunomiya, H. Shirato, and K. Ogasawara, "Differences in CT perfusion maps generated by different commercial software: Quantitative analysis by using identical source data of acute stroke patients 1," *Radiology*, vol. 254, no. 1, pp. 200–209, 2010.

[5] F. Calamante, D. L. Thomas, G. S. Pell, J. Wiersma, and R. Turner, "Measuring cerebral blood flow using magnetic resonance imaging techniques," *J Cerebr Blood F Met*, vol. 19, no. 7, pp. 701–735, 1999.

[6] N. Thacker, M. Scott, and A. Jackson, "Can dynamic susceptibility contrast magnetic resonance imaging perfusion data be analyzed using a model based on directional flow?," *J Magn Reson Im*, vol. 17, no. 2, pp. 241–255, 2003.

[7] S. Sourbron, "A tracer-kinetic field theory for medical imaging," *IEEE Trans Med Imaging*, 2014.

[8] F. Calamante, P. J. Yim, and J. R. Cebral, "Estimation of bolus dispersion effects in perfusion MRI using image-based computational fluid dynamics," *Neuroimage*, vol. 19, no. 2, pp. 341–353, 2003.

[9] L. Østergaard, R. M. Weisskoff, D. A. Chesler, C. Gyldensted, and B. R. Rosen, "High resolution measurement of cerebral blood flow using intravascular tracer bolus passages. part i: Mathematical approach and statistical analysis," *Magn Reson Med*, vol. 36, no. 5, pp. 715–725, 1996.

[10] B. Abels, E. Klotz, B. Tomandl, S. Kloska, and M. Lell, "Perfusion CT in acute ischemic stroke: a qualitative and quantitative comparison of deconvolution and maximum slope approach," *Am J Neuroradiol*, vol. 31, no. 9, pp. 1690–1698, 2010.

[11] M. Straka, G. W. Albers, and R. Bammer, "Real-time diffusion-perfusion mismatch analysis in acute stroke," *J Magn Reson Imaging*, vol. 32, no. 5, pp. 1024–1037, 2010.

[12] A. Bivard, C. Levi, N. Spratt, and M. Parsons, "Perfusion CT in acute stroke: a comprehensive analysis of infarct and penumbra," *Radiology*, vol. 267, no. 2, pp. 543–550, 2013.

[13] S. P. Sourbron and D. L. Buckley, "Classic models for dynamic contrast-enhanced MRI," *NMR in Biomedicine*, vol. 26, no. 8, pp. 1004–1027, 2013.

[14] K. Miles, "Measurement of tissue perfusion by dynamic computed tomography," *Br J Radiol*, vol. 64, no. 761, pp. 409–412, 1991.

[15] E. Klotz and M. König, "Perfusion measurements of the brain: using dynamic CT for the quantitative assessment of cerebral ischemia in acute stroke," *Eur J Radiol*, vol. 30, no. 3, pp. 170–184, 1999.

[16] R. Wirestam, L. Andersson, L. Østergaard, M. Bolling, J.-P. Aunola, A. Lindgren, B. Geijer, S. Holtås, and F. Ståhlberg, "Assessment of regional cerebral blood flow by dynamic susceptibility contrast MRI using different deconvolution techniques," *Magn Reson Med*, vol. 43, no. 5, pp. 691–700, 2000.

[17] T. Boutelier, K. Kudo, F. Pautot, and M. Sasaki, "Bayesian hemodynamic parameter estimation by bolus tracking perfusion weighted imaging," *IEEE T Med Imaging*, vol. 31, no. 7, pp. 1381–1395, 2012.

[18] K. Mouridsen, K. Friston, N. Hjort, L. Gyldensted, L. Østergaard, and S. Kiebel, "Bayesian estimation of cerebral perfusion using a physiological model of microvasculature," *Neuroimage*, vol. 33, no. 2, pp. 570–579, 2006.

[19] M. Sasaki, K. Kudo, T. Boutelier, F. Pautot, S. Christensen, I. Uwano, J. Goodwin, S. Higuchi, K. Ito, and F. Yamashita, "Assessment of the accuracy of a bayesian estimation algorithm for perfusion CT by using a digital phantom," *Neuroradiology*, vol. 55, no. 10, pp. 1197–1203, 2013.

[20] O. Wu, L. Østergaard, R. M. Weisskoff, T. Benner, B. R. Rosen, and A. G. Sorensen, "Tracer arrival timing-insensitive technique for estimating flow in mr perfusion-weighted imaging using singular value decomposition with a block-circulant deconvolution matrix," *Magn Reson Med*, vol. 50, no. 1, pp. 164–174, 2003.

[21] L. Evans, *Partial differential equations*. Providence, Rhode Island: American Mathematical Society, 2nd ed., 1998.

[22] A. A. Chan and S. J. Nelson, "Simplified gamma-variate fitting of perfusion curves," in *ISBI*, pp. 1067–1070, IEEE, 2004.

[23] R. Rosencranz and S. A. Bogen, "Clinical laboratory measurement of serum, plasma, and blood viscosity," *Am J Clin Pathol*, vol. 125 Suppl, pp. 78–86, Jun 2006.

[24] T. Kenner, "The measurement of blood density and its meaning," *Basic Res Cardiol*, vol. 84, no. 2, pp. 111–124, 1989.